4-2016

Effect of the Spiroiminodihydantoin Lesion on Nucleosome Stability and Positioning

Erika Norabuena
Mount Holyoke College

Sara Barnes Williams
Mount Holyoke College

Margaret A. Klureza
Wellesley College

Liana J. Goehring
Wellesley College

Brian Gruessner
Smith College

See next page for additional authors

Authors
Erika Norabuena, Sara Barnes Williams, Margaret A. Klureza, Liana J. Goehring, Brian Gruessner, Mala L. Radhakrishnan, Elizabeth R. Jamieson, and Megan E. Núñez

Effect of the Spiroiminodihydantoin Lesion on Nucleosome Stability and Positioning

Erika Norabuena[†], Sara Barnes Williams[†], Margaret Klureza[§], Liana Goehring[§], Brian Gruessner[‡], Mala Radhakrishnan[§], Elizabeth R. Jamieson[‡], and Megan E. Núñez[§*]

† Department of Chemistry and Program in Biochemistry
Mount Holyoke College, South Hadley MA 01075

‡ Department of Chemistry and Program in Biochemistry
Smith College, Northampton MA 01063

§ Department of Chemistry and Program in Biochemistry
Wellesley College, Wellesley MA 02481

* to whom correspondence should be addressed: Department of Chemistry, Wellesley College, 106 Central Street, Wellesley MA 02481. Office phone: (781) 283-3028. mnunez@wellesley.edu

Abbreviations

ROS, reactive oxygen species; Sp, spiroiminodihydantoin; 8-oxoG, 7,8-dihydro-8-oxo-2’-deoxyguanosine; BER, base excision repair; PMSF, phenylmethylsulfonylfluoride; MD, molecular dynamics.

Abstract

DNA is constantly under attack by oxidants, generating a variety of potentially mutagenic covalently modified species including oxidized guanine base products. One such product is spiroiminodihydantoin (Sp), a chiral, propeller-shaped lesion that strongly destabilizes the DNA helix in its vicinity. Despite its unusual shape and effect on dsDNA, DNA duplexes containing the Sp lesion form stable nucleosomes when incubated with histone octamers. Indeed, among six different combinations of lesion location and stereochemistry, only two duplexes display decreased ability to form nucleosomes, and these only by ~25%; the other four are statistically indistinguishable from the control. Nonetheless, kinetic factors also play a role: when the histone proteins have less time during assembly of the core particle to sample both lesion-containing and normal DNA strands, they are more likely to bind the Sp lesion DNA as compared to during slower assembly processes that better approximate thermodynamic equilibrium. Using DNase footprinting and molecular modeling, we discovered that the Sp lesion has only small effects (±1-2 bp) on the translational position of the DNA within the nucleosome. Each diastereomeric pair of lesions has the same effect on nucleosome positioning but lesions placed at different locations behave differently, illustrating that the location of the lesion and not its shape serves as the primary determinant of the most stable DNA orientation.

DNA is constantly under attack from a variety of exogenous and endogenous agents that covalently modify its structure, potentially leading to permanent mutations, cancer, cellular aging, or apoptosis (*1*). Reactive oxygen species (ROS) generated during cellular respiration, including peroxide, superoxide, and hydroxyl radicals, are particularly abundant, but radiation, heavy metals, organic oxidants, and inflammation-induced ROS all contribute to oxidation of cellular biomolecules (*2,3*). Within DNA, guanine bases are often the target of oxidation since they have the lowest redox potential of the four DNA bases (*4*). Indeed, it appears that thousands of guanine bases are oxidized in every mammalian cell, generating a variety of products including 8-oxoguanine (8oxoG) (*5,6*). 8oxoG is nearly identical in size, shape, and hydrogen-bonding partners to a normal guanine base, generating minimal disruption in the surrounding double helix (*7,8*). However, 8oxoG is even more easily oxidized than guanine itself, leading to the formation of a variety of secondary products including the spiroiminodihydantoin (Sp) lesion (*9-11*).

Unlike the 8oxoG lesion, the Sp lesion is not planar. Instead, it is shaped like a propeller, with its two rings connected at nearly right angles via a central chiral carbon. Both the R and S diastereomers can be formed in DNA. Not surprisingly given their unusual shape, both Sp lesions strongly destabilize the DNA duplex thermodynamically (*12-15*). Molecular dynamics simulations predict that neither stereoisomer should intercalate normally (*16*). Depending on the diastereomer and base pairing partner modeled, the most stable final structures include the lesion in the *syn* conformation with the B ring lying in the major groove, as well as *anti* conformations with one ring of the lesion lying in either groove. The only X-ray structure of Sp shows the S diastereomer of

the lesion bound to DNA polymerase β. The lesion takes on the *syn* conformation with the B ring in the major groove, and it distorts the nearby backbone (*17*). MD simulations predict and NMR studies confirm disruption of stacking and hydrogen bonding in the base pairs immediately flanking the lesion (*15,16*).

Formation of the Sp lesion in DNA is potentially mutagenic. Though Sp presents a rather strong block to DNA polymerization, it can be bypassed *in vitro* and *in vivo* by insertion of adenine and guanine on the opposite strand instead of the desired cytosine (*12,18*). The bypass thus leads to G⇒T and G⇒C transversion mutations. Fortunately, a variety of base excision repair glycosylases have evolved to recognize and efficiently remove the Sp lesion from DNA. Fpg (MutM), endonuclease III (Nth), and endonuclease VIII (Nei) in *E. coli*, OGG1 and OGG2 in yeast, and NEIL1 in mammals have all been shown to excise Sp from double stranded DNA (*19-24*). In many cases the excision occurs when Sp is paired to bases other than cytosine, providing a mechanism for the permanent transversion mutation to occur. In contrast, hOGG and MutY do not cleave Sp nor its complement. Supporting the critical role of BER proteins in specific removal of oxidized guanines *in vivo*, chromate oxidation of Nei-deficient *E. coli* leads to accumulation of Sp, but $MutM^-/MutY^-$ mutants accumulate 8oxoG instead (*22*). NEIL2 has been shown to remove Sp and other oxidized bases from single stranded DNA (*20*), supporting its proposed role in transcription coupled BER (*25*). Nucleotide excision repair can also remove Sp, providing a back-up mechanism for the removal of this disruptive lesion (*26,27*).

Though the Sp lesion has been well characterized in bare double stranded DNA, the DNA in human cells is highly complexed with many structural and regulatory proteins

that are likely to affect both the formation and repair of the Sp lesion *in vivo*. The next step in understanding Sp lesion mutagenicity lies in elucidating these quaternary interactions, beginning with the most abundant and fundamental protein partners.

The nucleosome is lowest order of packaging of the human genome, wherein ~150 base pairs of DNA are wrapped twice around an octameric core of histone proteins (*28-31*). A series of histone cores are bound along the DNA, yielding a "beads on a string" structure that compacts the DNA by about seven times. In addition to their function in structural compaction, nucleosomes also play a dynamic role in genome maintenance and expression by sequestering critical gene sequences from or exposing them to repair proteins, transcription factors, and RNA polymerase (*32-33*). Conversely, the structure of the DNA can affect the stability and structure of the nucleosome assembly (*34,35*). Here we explore how the Sp lesion influences the packaging of DNA into nucleosome core particles in order to determine whether the distortion in the double helix generated by the lesion alters the overall stability and conformation of a nucleosome.

Experimental Procedures

The general design and preparation of nucleosome core particles containing site-specifically incorporated DNA damage was reviewed recently by J.-S. Taylor (*36*).

Preparation of DNA Strands. The 146 base pair DNA duplex was constructed by ligation of smaller purified deoxyribonucleotides (Fig. S1). The DNA oligonucleotides were prepared commercially by phosphoramidite synthesis (Integrated DNA Technologies). The DNA strands were purified either by HPLC (1A, 1B, 1C, 2A, 2C, 2comp) or polyacrylamide gel electrophoresis in a 12% denaturing gel (2B, 1comp). HPLC purification was achieved on a reversed phase C18 column (Agilent Technologies) utilizing a gradient of 4-30% acetonitrile and 96-70% 25 mM ammonium acetate pH 7. The purified strands were then lyophilized, resuspended, and dialyzed in 1 kDa dialysis tubes (GE Healthcare) against 1 L of 1x TE (10 mM Tris HCl pH 7.8, 1 mM EDTA).

1B and 2B strands containing the Sp lesion were prepared from oligonucleotides containing the 8-oxoG lesion at the intended Sp location (Midland Certified Reagent Company). The oligonucleotides were oxidized with sodium hexachloroiridate(IV) hexahydrate ($Na_2IrCl_6 \bullet H_2O$) using the temperature-dependent method of Burrows and colleagues (*12,14*). After heating 12 μM 8-oxoG containing nucleotide in 10 mM sodium phosphate buffer (pH 7) and 100 mM NaCl with 100 μM Na_2IrCl_6 at 65˚C for 30 minutes, the reaction was quenched with EDTA (20 mM, pH 8) and desalted. The oligonucleotides containing the two diastereomers of the Sp lesion were purified by anion exchange chromatography using a Dionex DNAPac PA-100 9 x 250 mm column running at 2.5 mL/min. The various oligonucleotide products were separated using a 30 min long linear gradient beginning with 60% solution A (10% acetonitrile in 90% water)/40%

solution B (10% acetonitrile in 90% 1.5 M ammonium acetate buffer pH 6) and ending with 100% solution B.

Our experience from making several Sp-modified oligonucleotides under these conditions is that the Sp-modified oligonucleotides characteristically elute as two, sharp closely spaced peaks toward the end of the gradient (*13,14*). For both 1B sequences, the two diastereomers of the Sp lesion eluted at approximately ~25 and ~26 minutes, respectively. Each strand was named according to the position of the lesion and the order of elution, such that the first diastereomer to elute with the lesion at position 12 was called 12-1, etc. The 2B sequence also showed the characteristic two peaks, but in this case diastereomers eluted at ~28 and ~29 minutes, respectively. By comparison to the stereochemical characterization of Fleming *et al*., we expect that the diastereomer that elutes first is likely S and diastereomer that elutes second is likely R (*37*). To confirm that these samples had reacted similarly to our previous preparation of Sp oligos, masses for both diastereomers of each lesion-containing oligonucleotide were confirmed by ESI mass spectrometry. Characterization data, including representative HPLC chromatograms and mass spectral results, are included in Supplemental Materials (Fig. S2).

The concentration of all purified strands was measured spectrophotometrically at 260 nm, using the following molar extinction coefficients (ε_{260}): 1A=618300 M^{-1} cm^{-1}; 1B=179900 M^{-1} cm^{-1} ; 1C=619700 M^{-1} cm^{-1}, 2A=651900 M^{-1} cm^{-1}; 2B=204300 M^{-1} cm^{-1}, 2C=577600 M^{-1} cm^{-1}, 1comp=370200 M^{-1} cm^{-1}; 2comp=372100 M^{-1} cm^{-1}. The individual component strands were then ligated together as shown in Figure S1, forming a full-length, single-stranded 146 nucleotide oligomer (either containing the Sp lesion at

one of three locations or as a lesion-free control). Component DNA strands were combined to a 6 μM concentration with respect to each strand in a final volume of 500 μL and annealed at 90 ºC, then allowed to cool slowly to 16 ºC. The annealed strands were incubated with 4 μL of high-concentration T4 DNA ligase (2,000,000 U/mL, New England BioLabs) at 16 ºC overnight, followed by a second overnight incubation with a fresh addition of 4 μL ligase.

The full-length 146 nt DNA was separated from the shorter complementary template, unligated DNA, and singly ligated DNA by polyacrylamide gel electrophoresis in an 8% denaturing gel. The full-length band was visualized by UV shadowing and isolated from the gel using the crush-and-soak method. DNA was then desalted using Sep-Pak C18 columns (Waters), dried down, and resuspended in 1x TE. The concentration of each strand was determined spectrophotometrically at 260 nm, using extinction coefficients of 1,417,900 M^{-1} cm^{-1} for strand 1 and 1,433,800 M^{-1} cm^{-1} for strand 2. The integrity and sequence of the 146 nt single strands and the location of the lesions was confirmed by Maxam-Gilbert purine- and pyrimidine-specific sequencing reactions (Fig. S3). Each lesion was observed as a slightly enhanced band in the purine but not the pyrimidine lanes, confirming its location in the former case and its general integrity and robustness in the latter.

Radiolabeling of DNA. DNA was labeled at the 5' terminus by incubation with T4 Polynucleotide Kinase (New England BioLabs) and 50 μCi ^{32}P-ATP (Perkin-Elmer) at 37 ºC. Unincorporated mononucleotides were removed using disposable C18 reversed phase columns and the DNA was dried down on a centrifugal evaporator. The labeled DNA strands were quantitated on a scintillation counter using Cerenkov counting.

Duplex Preparation The labeled DNA was resuspended in buffer (10 mM Tris, 0.2 mM EDTA, 0.5 mM PMSF, and 0.01% Nonidet) containing 2 M NaCl. Additional unlabeled DNA and complementary strand were added to achieve a final concentration of 200 nM duplex. The DNA was then annealed by heating in a 90 ºC heat block and allowing to cool slowly to room temperature.

Isolation of Histones from Chicken Erythrocytes. Histones were isolated from chicken erythrocytes as nucleosome core particles (octamers of histones 2A, 2B, 3 and 4 with wrapped DNA) using established techniques (*38-41*). In short, chicken whole blood in sodium citrate (Pel-Freez Biologicals) was centrifuged at 5000xg at 5 ºC for 10 min. The supernatant (plasma) was discarded, the cell pellet was resuspended in buffer, and the solution was centrifuged for another 10 minutes. The centrifugation and resuspension was repeated until the supernatant lost most of its red color.

The cell pellet was then lysed in a hypotonic solution and centrifuged again to separate the nuclei from cell debris. The nuclei were rinsed thoroughly with buffer followed by centrifugation as above, supplemented with 2 mM calcium chloride, and digested with micrococcal nuclease at 37 ºC. After the suspended chromatin was separated from the nuclear debris by centrifugation, NaCl was added dropwise to a final concentration of exactly 0.65 M to release linker histones and other weakly-bound proteins from the DNA. Mono- and multi-nucleosomes were separated from smaller proteins using a Sepharose 4B size-exclusion column (Sigma Aldrich). Fractions containing histones were identified spectrophotometrically at 260 nm, as the DNA-wrapped histones showed a characteristic absorbance at that wavelength. These fractions were then pooled, dialyzed against buffer, and concentrated using Amicon 3000 MWCO

centrifugal filters (Millipore) where necessary. The purity and size of the isolated histones were confirmed by SDS PAGE, and the concentration of the isolated histones was approximated using a Bradford Coomassie protein assay (Thermo Scientific). Nucleosomes were stored in 50% glycerol at -20˚C until used.

Histone Exchange 10 μL of concentrated histones (~3 mg/mL) were combined with 30 μL radiolabeled DNA duplex samples (200 nM) in 2 M NaCl and incubated at 4˚C for 30 minutes. At this high salt concentration, nucleosomes disassemble. In the original single dialysis conditions, these histone/DNA samples were allowed to reassemble during dialysis against 1x TE, 200 μM PMSF in the cold room. In the double dialysis conditions, the dialysis tube was placed into a compartment containing 300 mL 1x TE with 600 mM NaCl, which itself was simultaneously dialyzed against a larger surrounding 3L container of 1x TE with no salt. The buffer in the outer beaker was changed three times over 36 hours.

Gel Shift to Quantify Nucleosome Formation Dialyzed histone exchange samples were run on a 5% non-denaturing polyacrylamide gel at 500 V for 3.5 hours to separate bound and unbound DNA. The gel was dried and then exposed to a phosphorimaging plate for 2.5 hours. The plate was scanned on a Molecular Dynamics Storm 820 phosphorimager (Amersham), and the bands were quantified using ImageQuant software. The nucleosome binding efficiency was calculated as the fraction bound relative to the total (after subtraction of background). Statistical significance was assessed using pairwise student's t-tests to compare means or F-tests to compare standard deviations.

DNase I Footprinting. Dialyzed histone exchange samples were concentrated using Amicon filters. Either concentrated histone exchange samples or bare DNA (as a control)

were combined with bovine pancreatic DNase I (New England Biolabs) and incubated at 37 ºC. Incubation times (0-12 min) and DNase dilutions (100-5000-fold) were adjusted to achieve <1 cut per duplex. The reaction was then halted by the addition of stop solution (50 mM EDTA in 50% glycerol for the nucleosomal samples; 100 mM EDTA and 2 mg/mL calf thymus DNA for the bare DNA samples). Bare DNA samples were then ethanol precipitated.

Exchange samples were run on a 5% nondenaturing polyacrylamide gel for 3.5 hours. The various bound and unbound DNA samples were identified by exposure to film in a darkroom setting, isolated from the preparatory polyacrylamide gel by the crush-and-soak method, and subsequently filtered through 0.45 μm and Amicon 3000 NMWL centrifugal filters (Millipore) to remove remaining gel fragments and borate, respectively. SDS was added to each sample to 0.01% (w/v), and the samples were incubated at 90 ºC for ten minutes. Finally, the DNA samples were extracted with phenol and chloroform and then precipitated with ethanol and ammonium acetate. DNA fragments were separated by denaturing PAGE in a 6-8% gel. The gel was dried and then exposed to a phosphorimager plate for 16-48 hours before scanning on a Molecular Dynamics Storm 820 phosphorimager (Amersham).

Because of the large number of preparative steps involved in this procedure, the signal to noise ratio in the gels was low and the salt content high, hindering our efforts at automated quantification and background subtraction. Instead, the sequence for each band in each lane had to be first assigned by comparison to the Maxam Gilbert purine- and pyrimidine-specific reactions run on every gel. Then, cleavage at each band was scored by visual inspection as either background, low, medium, or high. The results of a

dozen gels were then compiled and aligned in Excel, revealing clear and reproducible cleavage patterns with 10 bp periodicity characteristic of DNase I footprinting.

Visualization of Nucleosome Model Structures All nucleosome models are based upon the nucleosome structure published by Luger, Richmond and colleagues in 1997 (*42*). Coordinates were obtained from the Protein Data Bank (PDB ID 1AOI) and structures were examined in Swiss PDB Viewer (Swiss Institute for Bioinformatics).

Computational Modeling of Nucleosome-DNase I Interactions To clarify the correlation between DNase-mediated cleavage of histone-associated DNA and steric accessibility, computational models were generated for DNase/DNA/histone complexes at each potential DNA cleavage site along a model 146-bp ds DNA sequence. Interaction energies between the DNase I and the DNA/histone complex were then computed for each model to assess whether steric clashes would prohibit cleavage at the corresponding site.

As the starting point for each model, a crystal structure of DNase I bound to an 8-bp DNA segment (PDB ID 2DNJ) was fit to a specific portion of the crystal structure of 146-bp DNA segment wound around a histone (PDB ID 1AOI) (*42,43*). Specifically, for each value of *n* between 1-142, the phosphate atoms of bases B303-B307 and C310-C314 of 2DNJ were fit to bases $I_n - I_{n+4}$ and $J_{289-n} - J_{293-n}$ respectively of 1AOI (or $J_{289-n} - J_{293-n}$ and $I_n - I_{n+4}$, to simulate cleavage in the opposite orientation on the DNA). Structure fitting was carried out using ProFit v3.1 (*44*). After fitting, the DNA from the DNAase I structure was eliminated, and the resulting complex was minimized to eliminate minor steric clashes. Prior to minimization, disordered histone protein "tails" farther than 3.2 Å from any non-contiguous histone protein or DNA atoms and not part of secondary

structure elements were removed, except for the first of such residues at each tail. All water molecules and Mn^{2+} ions were also removed, as was the partially-resolved carbohydrate moiety attached to Asn18 of the DNase I. Hydrogen atoms were built in, and backbone adjacent to missing or removed residues was capped with neutral acetyl or n-methylamide groups. All structure preparation work was carried out using the CHARMM software package (*45*) and the charmm27 force field for protein and nucleic acids (*46-49*), with hydrogens built via the HBUILD facility (*50*).

Minimizations were carried out using the adopted-basis Newton-Raphson (ABNR) method in CHARMM. 250 minimization steps were used to relieve any relatively minor clashes resulting from fitting while retaining major clashes that would indicate an inaccessible DNA cleavage site. Only DNase residues and DNA bases with at least one atom within 7 Å of the DNase-DNA binding interface were allowed to relax in the minimization. As our focus was on steric clashes, a nonbonded switching function was used with a cutoff of 29 Å. A distance-dependent "4r" dielectric was used for electrostatics. Following each minimization, interaction (electrostatic and van der Waals) energies using the above cutoff were computed between the DNase and DNA/histone complex and are reported as a function of the approximate base pair closest to either "HD2" atom on DNase residues His134 and His252, residues known to be involved in cleavage (*51*). Sample model structures are shown in Supplemental Materials for DNase bound to an accessible and inaccessible portion of the DNA (Fig. S4).

Results and Discussion

Design and Assembly of the Nucleosome Complexes

To examine the effect of the Sp lesion on the stability and positioning of nucleosomes, we exchanged histone octamers onto 146-base pair DNA oligonucleotide duplexes to form nucleosome core particles. An Sp lesion was placed site-specifically at one of three locations, here called Lesions 7, 9, and 12, with cytosine complements mimicking the initial Sp-C base pair formed by guanine oxidation before any downstream mispairing by DNA polymerases (Fig. 1 a). Each lesion was chromatographically isolated in both diastereomeric forms, indicated by the second number in each sequence name (i.e. sequences 7-1 and 7-2). Thus, including the undamaged control DNA, seven different nucleosomes were produced.

The sequence of the 146 base pair duplex is non-palindromic to permit ligation of the single strands. The first 67 base pairs are identical to the human α-satellite sequence used by Luger and colleagues in their crystal structure to encourage uniform positioning (*42*). The last 60 nucleotides were flipped to the complementary sequence to obtain the sequence previously characterized by Lippard and colleagues with cisplatin (*52*). Each 146-nucleotide single strand was assembled by ligation of three smaller pieces of DNA, one of which included the Sp lesion (Fig S1). After purification, the two complementary146 nt strands were annealed to produce a 146 bp duplex.

Histone octamers isolated from chicken erythrocytes were exchanged from the chicken DNA onto radiolabeled 146-mer duplexes to produce nucleosome core particles by incubation in salt followed by dialysis. By analogy to the Luger crystal structure (1AOI) we hypothesized that the lesions would be located near the dyad axis adjacent to

the histone H3-H4 tetramer (Fig. 1 b,c). In fact because the DNA in the Luger sequence is pseudopalindromic, two slightly different models are possible, offset by ~1 bp, based on how we overlay the sequence onto the structure. If the lesions did not shift the positioning of the DNA, all three lesions would be located on the face of the DNA helix proximal to the protein octamer, but each in a slightly different orientation with correspondingly different flexibility and solution accessibility (Fig. 1 d,e).

Stability of Nucleosome Core Particles with the Sp Lesion

To determine the relative stability of nucleosome core particles with and without the Sp lesion, we measured quantitatively the exchange efficiency of the histone octamer from the original chicken DNA onto the seven 146 bp duplexes by gel shift. The 146 bp duplexes were radioactively labeled whereas the chicken DNA was not, so only the desired DNA was visible on the gel (Fig. 2 a). At 200 nM duplex, approximately 1/4 to 1/3 of the DNA outcompeted the chicken DNA to bind to the protein while the rest remained unbound, close enough to the K_d to allow us to measure small changes in the intensity of either band.

Like other researchers studying other DNA modifications or sequences, we initially observed that the slower-migrating band corresponding to the nucleosomes was broad, blurry, and looked to contain two species, likely representing slightly different conformational states (Fig 2 a) (*53,54*). Following the advice of Widom and colleagues (*55*), we altered the exchange procedure to slow the assembly step by using a double dialysis, allowing the particles time to converge on a single thermodynamically-favored state. Interestingly, the "slow" double dialysis procedure had no effect on the exchange

efficiency of the undamaged control DNA, except to favor the formation of a single nucleosome band and to reduce variation between experiments. However, slow dialysis *decreased* the efficiency of nucleosome formation on the DNA containing lesion 12 (Fig. 2 b). In other words, when the histone cores were allowed more time to sample both damaged and undamaged DNA, they were less likely to bind the lesion DNA than when the nucleosome collapsed quickly due to rapidly plummeting salt concentrations. This kinetic sampling is most likely to occur during the binding of the H3-H4 tetramer, which occurs at relatively high salt concentrations as the first step in nucleosome assembly (*56,57*). Since the Sp lesion is located proximal to the tetramer in the final nucleosome structure, this step would be directly influenced by the presence of the lesion. Once the salt concentration drops, the H2A/H2B dimers bind to form an octamer, and the DNA is largely wrapped around it. The DNA retains sufficient mobility to slide around the nucleosome surface (*54*) but would have a higher activation energy to completely disassemble and reassemble on a different piece of DNA.

Next we measured the efficiency of nucleosome assembly on all seven duplexes, i.e. the control and both diastereomers of all three lesions, under the slower assembly conditions dictated by the double dialysis (Fig. 3 a). Surprisingly, the efficiency of assembly was relatively conserved when the Sp lesion was present (Fig. 3 b). Only in two cases, Lesion 7-1 and Lesion 12-1, did the binding diminish to a statistically-significant extent relative to control DNA, whereas their respective diastereomers and lesion 9 bound equally well as the control DNA. Thus it appears that the nucleosome structure is able to accommodate the Sp lesion. DNA duplexes 7-1 and 12-1 are quite similar to one another structurally, which may explain their thermodynamic similarity:

the lesions are located at nearly mirror image positions in the structure (Fig. 1 d), facing "in" toward the protein, and both likely have the same S stereochemistry (*37*). For comparison, benzopyrene diol epoxide (BPDE) damage products have been shown to increase the efficiency of nucleosome formation, while UV photoproducts including the thymine dimer decrease nucleosome formation efficiency only somewhat, confirming the ability of the nucleosome to form around non-canonical DNA lesions (*58,59*).

DNase I Footprinting to Determine Control DNA Position in the Nucleosome Core Particle

The gel shift experiments indicate that the nucleosome structure is able to accommodate the Sp lesion in some fashion, leading us to inquire about the positioning of the DNA helix within the particle. First, we used DNase I footprinting to map the position of the undamaged control DNA duplex relative to the histone octamer core to determine whether the model of Luger *et al*. was indeed representative of our DNA assemblies despite the modification in sequence and the different source of histone proteins. The presence of the histone proteins reduces the intensity of DNase I cleavage throughout the DNA in absolute terms, but also changes the pattern, decreasing cleavage relatively at some sites and increasing it at others in a periodic fashion (Fig. 4 a). This behavior confirms that the DNA is bound in a nucleosome core particle. When these bands were mapped to the three-dimensional nucleosome core particle model, the locations of robust cleavage generally mapped to the outside face of the DNA and the locations of diminished cleavage to the inside face (Fig. 4 b,c). The positions of cleavage were conserved between singly- and doubly-dialyzed samples, and were internally

consistent between both radiolabeled strands. Some sites on the DNA are cleaved in neither the bound nor unbound states, reflecting the moderate intrinsic sequence preference of the nuclease.

To determine whether the model of Luger *et al*. accurately reflects the orientation of these nucleosomes at the base pair level, we predicted computationally the sites of DNase I cleavage on the nucleosome. At every nucleotide position, we aligned the structure of a cocrystallized DNase I-DNA complex (*43*) onto the nucleosome using the DNA as a guide. After briefly minimizing the conformations energetically, we then evaluated the interaction energy of each DNaseI-nucleosome complex. Complexes with large positive free energies displayed major steric clashes between proteins.

This steric modeling predicts the experimentally well-known oscillating cleavage pattern of footprinting agents on nucleosomes with a ~10 bp period (Fig. 5) (*29*). The modeling reveals that due to the size and asymmetry of this monomeric minor-groove binding nuclease, ≤ 4 nt (of 10 nt) are accessible for DNase cleavage on each strand within each turn of the helix. Note however that this model is "optimistic" in that it considers only whether given sites on the DNA are sterically accessible; it does not also incorporate the inherent sequence preference of the enzyme itself, caused by the enzyme's requirement for particular DNA conformations with favorable minor groove widths and sequence-dependent flexibility (*51*), nor interactions with the histone tails. These additional factors would be expected to modulate but not fundamentally change the sinusoidal shape of the curve.

The experimentally-observed cleaved and uncleaved sites generally map well onto the computational prediction (Fig. 5). The alignment of the two periodic patterns confirms

that the Luger model is indeed a fair representation of how this 146 bp DNA duplex forms a nucleosome with histone proteins. There are small discrepancies between our observed cleavage pattern and the predicted cleavage pattern, likely due to small but compounding factors: the two similar and possibly equivalent orientations of the nonpalindromic 146 bp DNA on the nucleosome; small (±1 bp) inaccuracies in assignment of cleavage sites on the gel; the enzyme's preference for/against cleaving particular sequences; interactions with the histone tails; and dynamic fluctuations in the nucleosome (*60*). Nonetheless there is no evidence of a widespread 5' or 3' skew that would indicate a misalignment between the model and the experimental system.

DNase I Footprinting to Determine Lesion DNA Position in the Nucleosome Core Particle

With a model of this nucleosome in hand, we characterized the positioning of the six lesion-containing DNA duplexes on the nucleosome core particle using DNase I footprinting (Fig. 6). Three major trends emerged from an analysis of multiple replicates performed under both single- and double-dialysis conditions:

(1) All of the lesion DNase I footprints are globally similar to the control and each other but with small alterations.

(2) Moderate to strong cleavage is observed near the lesion itself.

(3) Each diastereomeric pair displays matching footprints.

Despite the similarities in DNAase I footprints between all seven duplexes, there are small but notable effects of the lesion on the nucleosome structure. In the construct containing lesion 7, two bands located ~15 and 25 bp (1.5 and 2.5 helical turns) away

from the lesion reproducibly disappear, though bands immediately 3' to them do not, nor do most of the cleavage bands (Fig. 6 a,c). The most reasonable change consistent with this pattern is a subtle ~1 bp translational repositioning (Fig. S5). Such a small change would slide the lesion away along the DNA-histone interface by 36˚ but would not be sufficient to move it all the way to face the solution (Fig. 1; Fig. S6), which may account for the larger adverse thermodynamic effect of placing the lesion at this location (Fig. 3).

The construct containing Lesion 9 displays the largest number and severity of changes in footprints relative to the control (Fig. 6 a,d). Bands located ~27 bp and ~36 bp (2.7 and 3.6 helical turns) away from the lesion disappear, while a band 38 bp away is somewhat augmented. Examination of our computational model shows that a ~2 bp translational repositioning could explain the observed cleavage pattern, but in the opposite direction as for Lesion 7 (Fig. S5). This repositioning would rotate the DNA by ~ 72˚ to place the lesion further away from the histone core on the solution-exposed face (Fig. S6), perhaps explaining the absence of a thermodynamic effect on binding.

The construct containing the Sp lesion at position 12 also showed some changes in the footprint pattern relative to the control at 1.5 and 3.5 helical turns away from the lesion (Fig. 6 e) under single dialysis conditions, but the changes were quite subtle and seemed to be particularly sensitive to the rate of assembly *via* the rate of dialysis. Under double dialysis conditions, the footprint at sites distal from the lesion was not different than the control, although a DNase cleavage band near the lesion was observed regardless of assembly rate (Fig. 6b).

These observations together lead us to conclude that at equilibrium the final nucleosome structure balances the effects of length, native DNA sequence curvature, and

lesion placement, with the lesion playing a rather modest role. Translational positioning is a critical factor on a duplex this length. Because 146 bp is close to the minimum amount of DNA required to form a stable nucleosome in the absence of linker histones H1/H5, any translational sliding of the DNA along the edge of the octamer in either direction will result in a loss of DNA-histone contacts, and these losses would become more and more pronounced the more asymmetrically the DNA is bound to the core. This length effect would tend to center the DNA on the histone octamer, dictating a small set of thermodynamically-favored conformations with similar translational positions. In long genomic DNA this effect of the DNA ends would be lacking, but translational constraints could be imposed by the location of neighboring nucleosomes and the length of intervening linker DNA instead.

Secondly, within that set of translationally-favored states, any significant native curvature in the DNA sequence will favor particular rotational positions over others. The first half of this sequence is based on the human α-satellite DNA sequence, containing phased A-tracts that curve the DNA naturally even in the absence of nucleosomes. The second half of sequence is the complement of the first, which would also likely display significant native curvature though not in phase with the first. Danford *et al.* (2005) analyzed the positioning of the identical sequence on recombinant *Xenopus* histones using exonuclease III and hydroxyl radical footprinting and found it to be centrally bound on the core particle but somewhat weakly positioned, since the footprints on both gels were weaker and more blurry than when strongly positioned (*52*). Our DNase I footprinting of the control nucleosomes is consistent with centering the DNA translationally and phasing the DNA rotationally according to the human α-satellite

sequence, although equilibration between similar positions (within 1-2 bp) is certainly consistent with the resolution of our gels.

Most interesting is that the disruptive effect of the bulky, destabilizing Sp lesion is accommodated by sliding the lesion away from the histone surface by only 1-2 base pairs in either direction. Thus, in this system, the effect of the Sp lesion on nucleosome position appears to add a small "tweak" to translational concerns and sequence-dependent bending. Overall, the effect of Sp on position appears to be similar or slightly weaker than the thymine dimer (*61-63*) or cisplatin (*53,64*). Studies with different cisplatin lesions in varying sequences have revealed that lesion-induced deformation can override the effects of length and sequence-dependent bending; however, when placed in the same region of the same sequence as explored here, cisplatin intrastrand crosslinks cause the nucleosome to favor conformations that are very similar to what we observe with Sp (*52,65*).

Given our current tentative understanding of the structure of the diastereomeric Sp lesions in protein-free duplex DNA, it is difficult to predict yet the local DNA structure around an Sp lesion bound in a nucleosome. We observed that the DNA around the lesion appears to be cleaved by the nuclease, even in the case of Lesions 7 and 12 where this experimental footprinting and model of the control DNA conformation predict these sites to face inward toward the histone octamer (Fig. 1, Fig. S6). It may be that the equilibrium structure of the lesion-containing nucleosome encompasses local DNA distortions, whether by kinking the backbone or even flipping the chiral, propeller-shaped lesion from the otherwise aromatic π stack of the DNA. Alternatively, the lesion may cause this section of the DNA to be locally more dynamic than otherwise (*60*). Our third

general observation tells us that the *location* of the lesion is more far important than its shape in determining the final nucleosome conformation. Though both diasteromers have been shown to be quite disruptive to duplex stability (*12-15*), modeling predicts that they may protrude into different grooves of the helix (*16*). Thus it appears that the final nucleosome conformations involve moving the distortion to locations where a distorted DNA structure can be tolerated, rather than directly matching the shape of the distortion. Along that vein, here we examined the effect of the Sp-C base pair on nucleosome formation, but the Sp lesion is often paired with purines during replication. Sp-G or Sp-A base pairs might be more strongly positioning than Sp-C because they are larger, although conversely they do have a higher melting temperature (*14*). Given that the two Sp diastereomers appear to have identical effects on nucleosome positioning, we hypothesize that the exact shape of the Sp lesion base pair may not matter as far as positioning is concerned, but that remains to be demonstrated.

The ability of the Sp lesion to subtly shift nucleosome stability and positioning potentially has implications for genome regulation and maintenance. In the future we hope to learn whether the shape of the nucleosome produces geometric constraints that enhance or limit formation of either isomer of the Sp lesion, as has been seen for the thymine dimer lesion (*66*). Even if the nucleosome does not constrain Sp formation, by binding the lesion strongly nucleosomes may sequester Sp from proteins involved in the various repair pathways (*67-72*), thereby increasing the likelihood of permanent mutagenesis.

Conclusion

Duplex DNA containing the spiroiminodihydantoin lesion can be bound efficiently by histone proteins to form a nucleosome core particle, but the lesion has subtle effects on the stability and positioning of the nucleosome that may affect its own mutagenic potential.

Funding Sources

Funding for this work was provided by a National Institutes of Health AREA grant (National Cancer Institute, 1R15 CA149958-01A1) to MEN and ERJ, a Clare Boothe Luce Foundation professorship to MEN, a Henry Dreyfus Teacher-Scholar award to MEN, as well as the generosity of our institutions, Wellesley College, Mount Holyoke College, and Smith College.

Acknowledgements

The authors would like to express our deep gratitude to Ms. Hanyu (Esther) Shui for preliminary characterization of lesion 12, Ms. Raquel Hernandez-Solis for her contributions to nucleosome preparation, Dr. Cassandra Pattanayak of the Wellesley Quantitative Analysis Institute for her advice about statistical tests and Ms. Divya Satishchandra for rechecking them, and Dr. Kalina Dimova at the Smith College Center for Proteomics for her assistance with mass spectral characterization.

Supporting Information

Sequences of oligonucleotides use to assemble the 146 bp duplex; chromatograms, mass spectra, and Maxam-Gilbert sequencing of DNA containing Sp lesions; representative favorable and unfavorable modeled alignments of DNase I with nucleosomes; and graphical view of experimentally-determined DNase I footprint cleavage overlaid on binding model.

References

(1) Friedberg, E. C., Walker, G. C., Siede, W., Wood, R. D., Schultz, R. A., and Ellenberger, T. (2006) *DNA Repair and Mutagenesis* 2nd ed. ASM Press, Washington, D.C.

(2) Dedon, P. C. (2011) Oxidation and deamination of DNA by endogenous sources. In *Chemical Carcinogenesis: Current Cancer Research* (T.M. Penning, Ed.) pp. 209–225, Springer Science and Business Media.

(3) Evans, M. D., Dizdaroglu, M., and Cooke, M. S. (2004) Oxidative DNA damage and disease: induction, repair and significance. *Mutat. Res. 567*, 1–61.

(4) Steenken, S., and Jovanovic, S. (1997) How easily oxidizable is DNA? One-electron reduction potentials of adenosine and guanosine radicals in aqueous solution. *J. Am. Chem. Soc. 119*, 617–618.

(5) Helbock, H., Beckman, K., Shigenaga, M., Walter, P., Woodall, A., Yeo, H., and Ames, B. (1998) DNA oxidation matters: the HPLC-electochemical detection assay of 8-oxo-deoxyguanosine and 8-oxo-guanine. *Proc. Natl. Acad. Sci. USA 95*, 288–293.

(6) Collins, A. R., Cadet, J. A., Möller, L., Poulsen, H. E., and Viña, J. (2004) Are we sure we know how to measure 8-oxo-7,8-dihydroguanine in DNA from human cells? *Arch. Biochem. Biophys. 423*, 57–65.

(7) Lipscomb, L., Peek, M., Morningstar, M., Verghis, S., Miller, E., Rich, A., Essigmann, J., and Williams, L. (1995) X-ray structure of a DNA decamer containing 7,8-dihydro-8-oxoguanine. *Proc. Natl. Acad. Sci. USA 92*, 719–723.

(8) Crenshaw, C. M., Wade, J. E., Arthanari, H., Frueh, D., Lane, B. F., and Núñez, M. E. (2011) Hidden in plain sight: subtle effects of the 8-oxoguanine lesion on the structure, dynamics, and thermodynamics of a 15-base pair oligodeoxynucleotide duplex. *Biochemistry 50*, 8463–8477.

(9) Luo, W., Muller, J. G., Rachlin, E. M., and Burrows, C. J. (2001) Characterization of hydantoin products from one-electron oxidation of 8-oxo-7,8-dihydroguanosine in a nucleoside model. *Chem. Res. Toxicol. 14*, 927–938.

(10) Luo, W., Muller, J., Rachlin, E., and Burrows, C. (2000) Characterization of spiroiminodihydantoin as a product of one-electron oxidation of 8-oxo-7, 8-dihydroguanosine. *Org. Lett. 2*, 613–616.

(11) Slade, P. G., Hailer, M. K., Martin, B. D., and Sugden, K. D. (2005) Guanine-specific oxidation of double-stranded DNA by Cr (VI) and ascorbic acid forms spiroiminodihydantoin and 8-oxo-2'-deoxyguanosine. *Chem. Res. Toxicol. 18*, 1140–1149.

(12) Kornyushyna, O., Berges, A. M., Muller, J. G., and Burrows, C. J. (2002) In vitro nucleotide misinsertion opposite the oxidized guanosine lesions spiroiminodihydantoin and guanidinohydantoin and DNA synthesis past the lesions using *Escherichia coli* DNA polymerase I (Klenow fragment). *Biochemistry 41*, 15304–15314.

(13) Chinyengetere, F., and Jamieson, E. R. (2008) Impact of the oxidized guanine lesion spiroiminodihydantoin on the conformation and thermodynamic stability of a 15-mer DNA duplex. *Biochemistry 47*, 2584–2591.

(14) Gruessner, B., Dwarakanath, M., Martei, M., and Jamieson, E. R. (2016) Effect of base-pairing partner on the thermodynamic stability of the diastereomeric spiroiminodihydantoin lesion. *Chem. Res. Toxicol. 29,* 279-284.

(15) Khutsishvili, I., Zhang, N., Marky, L. A., Crean, C., Patel, D. J., Geacintov, N. E., and Shafirovich, V. (2013) Thermodynamic profiles and nuclear magnetic resonance studies of oligonucleotide duplexes containing single diastereomeric spiroiminodihydantoin lesions. *Biochemistry 52*, 1354–1363.

(16) Jia, L., Shafirovich, V., Shapiro, R., Geacintov, N. E., and Broyde, S. (2005) Structural and thermodynamic features of spiroiminodihydantoin damaged DNA duplexes. *Biochemistry 44*, 13342–13353.

(17) Eckenroth, B. E., Fleming, A. M., Sweasy, J. B., Burrows, C. J., and Doublié, S. (2014) Crystal structure of DNA polymerase β with DNA containing the base lesion spiroiminodihydantoin in a templating position. *Biochemistry 53*, 2075–2077.

(18) Henderson, P. T., Delaney, J. C., Muller, J. G., Neeley, W. L., Tannenbaum, S. R.,

Burrows, C. J., and Essigmann, J. M. (2003) The hydantoin lesions formed from oxidation of 7,8-dihydro-8-oxoguanine are potent sources of replication errors in vivo. *Biochemistry 42*, 9257–9262.

(19) Leipold, M. D., Workman, H., Muller, J. G., Burrows, C. J., and David, S. S. (2003) Recognition and removal of oxidized guanines in duplex DNA by the base excision repair enzymes hOGG1, yOGG1, and yOGG2. *Biochemistry 42*, 11373–11381.

(20) Hazra, T. K., Muller, J. G., Manuel, R. C., Burrows, C. J., Lloyd, R. S., and Mitra, S. (2001) Repair of hydantoins, one electron oxidation product of 8-oxoguanine, by DNA glycosylases of *Escherichia coli*. *Nuc. Acids Res. 29*, 1967–1974.

(21) Leipold, M., Muller, J., Burrows, C., and David, S. (2000) Removal of hydantoin products of 8-oxoguanine oxidation by the *Escherichia coli* DNA repair enzyme Fpg. *Biochemistry 39*, 14984–14992.

(22) Hailer, M. K., Slade, P. G., Martin, B. D., and Sugden, K. D. (2005) Nei deficient *Escherichia coli* are sensitive to chromate and accumulate the oxidized guanine lesion spiroiminodihydantoin. *Chem. Res. Toxicol. 18*, 1378–1383.

(23) Krishnamurthy, N., Muller, J. G., Burrows, C. J., and David, S. S. (2007) Unusual structural features of hydantoin lesions translate into efficient recognition by *Escherichia coli* Fpg. *Biochemistry 46*, 9355–9365.

(24) Krishnamurthy, N., Zhao, X., Burrows, C. J., and David, S. S. (2008) Superior removal of hydantoin lesions relative to other oxidized bases by the human DNA glycosylase hNEIL1. *Biochemistry 47*, 7137–7146.

(25) Banerjee, D., Mandal, S. M., Das, A., Hegde, M. L., Das, S., Bhakat, K. K., Boldogh, I., Sarkar, P. S., Mitra, S., and Hazra, T. K. (2011) Preferential repair of oxidized base damage in the transcribed genes of mammalian cells. *J. Biol. Chem. 286*, 6006–6016.

(26) McKibbin, P. L., Fleming, A. M., Towheed, M. A., Van Houten, B., Burrows, C. J., and David, S. S. (2013) Repair of hydantoin lesions and their amine adducts in DNA by base and nucleotide excision repair. *J. Am. Chem. Soc. 135*, 13851–13861.

(27) Shafirovich, V., Kropachev, K., Anderson, T., Liu, Z., Kolbanovskiy, M., Martin, B.

D., Sugden, K., Shim, Y., Chen, X., Min, J.-H., and Geacintov, N. E. (2016) Base and nucleotide excision repair of oxidatively generated guanine lesions in DNA. *J. Biol. Chem. 291*, 5309–5319.

(28) Kornberg, R. D. (1977) Structure of chromatin. *Ann. Rev. Biochem. 46*, 931–954.

(29) McGhee, J. D., and Felsenfeld, G. (1980) Nucleosome structure. *Ann. Rev. Biochem. 49*, 1115–1156.

(30) Ramakrishnan, V. (1997) Histone structure and the organization of the nucleosome. *Ann. Rev. Biophys. Biomol. Struct. 26*, 83–112.

(31) Andrews, A. J., and Luger, K. (2011) Nucleosome structure(s) and stability: variations on a theme. *Annu. Rev. Biophys. 40*, 99–117.

(32) Kaplan, N., Moore, I. K., Fondufe-Mittendorf, Y., Gossett, A. J., Tillo, D., Field, Y., LeProust, E. M., Hughes, T. R., Lieb, J. D., Widom, J., and Segal, E. (2009) The DNA-encoded nucleosome organization of a eukaryotic genome. *Nature 458*, 362–366.

(33) Jiang, C. Z., and Pugh, B. F. (2009) Nucleosome positioning and gene regulation: advances through genomics. *Nature Rev. 10*, 161–172.

(34) Segal, E., Fondufe-Mittendorf, Y., Chen, L., Thåström, A., Field, Y., Moore, I. K., Wang, J.-P. Z., and Widom, J. (2006) A genomic code for nucleosome positioning. *Nature 442*, 772–778.

(35) Albert, I., Mavrich, T. N., Tomsho, L. P., Qi, J., Zanton, S. J., Schuster, S. C., and Pugh, B. F. (2007) Translational and rotational settings of H2A.Z nucleosomes across the *Saccharomyces cerevisiae* genome. *Nature 446*, 572–576.

(36) Taylor, J.-S. (2015) Design, synthesis, and characterization of nucleosomes containing site-specific DNA damage. *DNA Repair 36*, 59–67.

(37) Fleming, A. M., Orendt, A. M., He, Y., Zhu, J., Dukor, R. K., and Burrows, C. J. (2013) Reconciliation of chemical, enzymatic, spectroscopic and computational data to assign the absolute configuration of the DNA base lesion spiroiminodihydantoin. *J. Am. Chem. Soc. 135*, 18191–18204.

(38) Lutter, L. C. (1989) Digestion of nucleosomes with deoxyribonucleases I and II. *Meth. Enzymol. 170*, 264–269.

(39) Lutter, L. C. (1978) Kinetic analysis of deoxyribonuclease I cleavages in the nuclesome core: evidence for a DNA superhelix. *J. Mol. Biol. 124*, 391–420.

(40) Drew, H. R., and Callidine, C. R. (1987) Sequence-specific positioning of core histones on an 860 base-pair DNA: experiment and theory. *J. Mol. Biol. 195*, 143–173.

(41) Kornberg, R. D., LaPointe, J. W., and Lorch, Y. (1989) Preparation of nucleosomes and chromatin. *Meth. Enzymol. 170*, 3–14.

(42) Luger, K., Mader, A., Richmond, R., Sargent, D., and Richmond, T. (1997) Crystal structure of the nucleosome core particle at 2.8 Å resolution. *Nature 389*, 251–260.

(43) Lahm, A., and Suck, D. (1991) DNase I-induced DNA conformation. 2 Å structure of a DNase I-octamer complex. *J. Mol. Biol. 222*, 645–667.

(44) McLachlan, A. D. (1982) Rapid comparison of protein structures. *Acta Crystallogr. A38*, 871–873.

(45) Brooks, B. R., Bruccoleri, R. E., Olafson, B. D., States, D. J., Swaminathan, S., and Karplus, M. (1983) CHARMM: A program for macromolecular energy, minimization, and dynamics calculations. *J. Comp. Chem. 4*, 187–217.

(46) Mackerell, A. D., Bashford, D., Bellott, M., Dunbrack, R. L., colleagues. (1998) All-atom empirical potential for molecular modeling and dynamics studies of proteins. *J. Phys. Chem. 102*, 3586–3616.

(47) Foloppe, N., and MacKerell, A. D., Jr. (2000) All-atom empirical force field for nucleic acids: I. Parameter optimization based on small molecule and condensed phase macromolecular target data. *J. Comp. Chem. 21*, 86–104.

(48) Mackerell, A. D., and Banavali, N. K. (2000) All-atom empirical force field for nucleic acids: II. Application to molecular dynamics simulations of DNA and RNA in solution. *J. Comp. Chem. 21*, 105–120.

(49) Mackerell, A. D., Jr., Feig, M., and Brooks, C. L., III. (2004) Extending the

treatment of backbone energetics in protein force fields: Limitations of gas-phase quantum mechanics in reproducing protein conformational distributions in molecular dynamics simulations. *J. Comp. Chem. 25*, 1400–1415.

(50) Brünger, A. T., and Karplus, M. (1988) Polar hydrogen positions in proteins: empirical energy placement and neutron diffraction comparison. *Proteins: Struct., Funct., Bioinf. 4*, 148–156.

(51) Suck, D. (1994) DNA recognition by DNase I. *J. Mol. Recognit. 7*, 65–70.

(52) Danford, A. J., Wang, D., Wang, Q., Tullius, T. D., and Lippard, S. J. (2005) Platinum anticancer drug damage enforces a particular rotational setting of DNA in nucleosomes. *Proc. Natl. Acad. Sci. USA 102*, 12311–12316.

(53) Ober, M., and Lippard, S. J. (2007) Cisplatin damage overrides the predefined rotational setting of positioned nucleosomes. *J. Am. Chem. Soc 129*, 6278–6286.

(54) Luger, K. (2003) Structure and dynamic behavior of nucleosomes. *Curr. Opin. Genet. Dev. 13*, 127–135.

(55) Thåström, A., Lowary, P. T., and Widom, J. (2004) Measurement of histone–DNA interaction free energy in nucleosomes. *Methods 33*, 33–44.

(56) Luger, K., Dechassa, M. L., and Tremethick, D. J. (2012) New insights into nucleosome and chromatin structure: an ordered state or a disordered affair? *Nat. Rev. Mol. Cell Biol. 13*, 436–447.

(57) Bohm, V., Hieb, A. R., Andrews, A. J., Gansen, A., Rocker, A., Toth, K., Luger, K., and Langowski, J. (2011) Nucleosome accessibility governed by the dimer/tetramer interface. *Nuc. Acids Res. 39*, 3093–3102.

(58) Mann, D. B., Springer, D. L., and Smerdon, M. J. (1997) DNA damage can alter the stability of nucleosomes: effects are dependent on damage type. *Proc. Natl. Acad. Sci. USA 94*, 2215–2220.

(59) Kosmoski, J. V., and Smerdon, M. J. (1999) Synthesis and nucleosome structure of DNA containing a UV photoproduct at a specific site. *Biochemistry 38*, 9485–9494.

(60) Li, G., Levitus, M., Bustamante, C., and Widom, J. (2004) Rapid spontaneous

accessibility of nucleosomal DNA. *Nat. Struct. Mol. Biol. 12*, 46–53.

(61) Suquet, C., and Smerdon, M. J. (1993) UV damage to DNA strongly influences its rotational setting on the histone surface of reconstituted nucleosomes. *J. Biol. Chem. 268*, 23755–23757.

(62) Schieferstein, U., and Thoma, F. (1996) Modulation of cyclobutane pyrimidine dimer formation in a positioned nucleosome containing poly(dA.dT) tracts. *Biochemistry 35*, 7705–7714.

(63) Kosmoski, J. V., Ackerman, E. J., and Smerdon, M. J. (2001) DNA repair of a single UV photoproduct in a designed nucleosome. *Proc. Natl. Acad. Sci. USA 98*, 10113–10118.

(64) Ober, M., and Lippard, S. J. (2008) A 1,2-d(GpG) cisplatin intrastrand cross-link influences the rotational and translational setting of DNA in nucleosomes. *J. Am. Chem. Soc. 130*, 2851–2861.

(65) Todd, R. C., and Lippard, S. J. (2010) Consequences of cisplatin binding on nucleosome structure and dynamics. *Chem. Biol. 17*, 1334–1343.

(66) Gale, J. M., Nissen, K. A., and Smerdon, M. J. (1987) UV-induced formation of pyrimidine dimers in nucleosome core DNA is strongly modulated with a period of 10.3 bases. *Proc. Natl. Acad. Sci. USA 84*, 6644–6648.

(67) Hara, R., Mo, J., and Sancar, A. (2000) DNA damage in the nucleosome core is refractory to repair by human excision nuclease. *Mol. Cell. Biol. 20*, 9173–9181.

(68) Beard, B. C., Wilson, S. H., and Smerdon, M. J. (2003) Suppressed catalytic activity of base excision repair enzymes on rotationally positioned uracil in nucleosomes. *Proc. Natl. Acad. Sci. USA 100*, 7465–7470.

(69) Prasad, A., Wallace, S. S., and Pederson, D. S. (2007) Initiation of base excision repair of oxidative lesions in nucleosomes by the human, bifunctional DNA glycosylase NTH1. *Mol. Cell. Biol. 27*, 8442–8453.

(70) Jagannathan, I., Cole, H. A., and Hayes, J. J. (2006) Base excision repair in nucleosome substrates. *Chromosome Res. 14*, 27–37.

(71) Odell, I. D., Newick, K., Heintz, N. H., Wallace, S. S., and Pederson, D. S. (2010) Non-specific DNA binding interferes with the efficient excision of oxidative lesions from chromatin by the human DNA glycosylase, NEIL1. *DNA Repair 9*, 134–143.

(72) Hinz, J. M., Rodriguez, Y., and Smerdon, M. J. (2010) Rotational dynamics of DNA on the nucleosome surface markedly impact accessibility to a DNA repair enzyme. *Proc. Natl. Acad. Sci. USA 107*, 4646–4651.

Figures

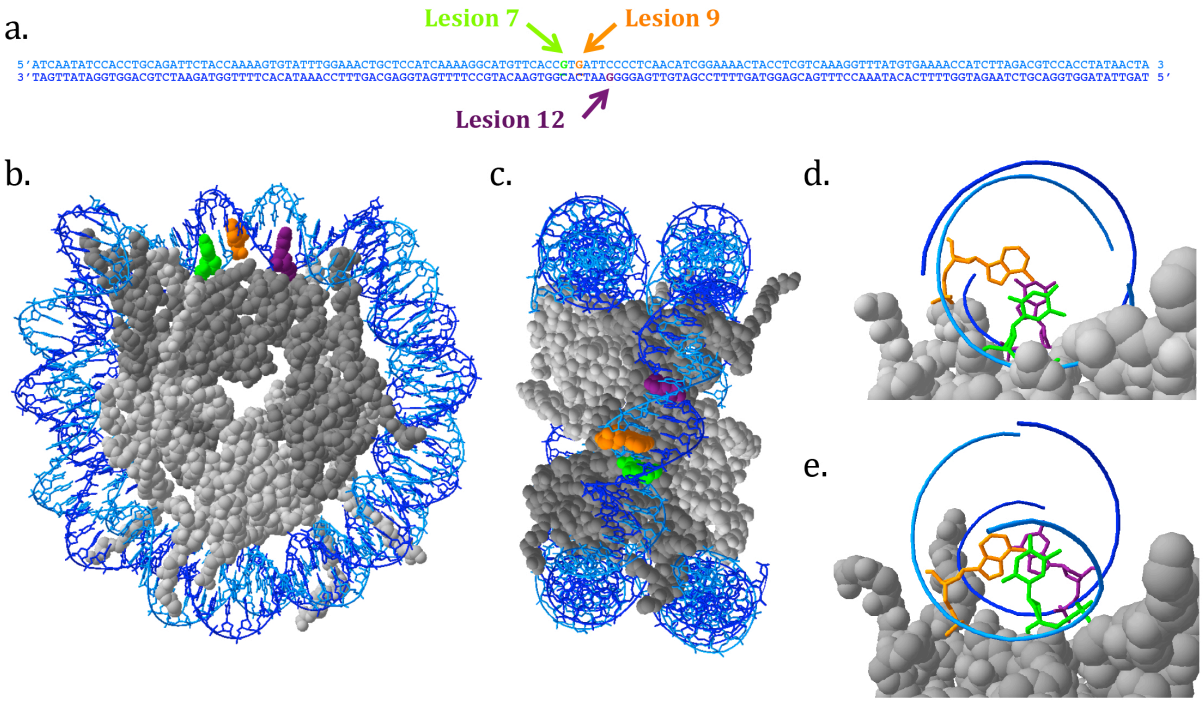

Figure 1: *Sequence and Starting Model of the Nucleosome Core Particle*. (a) Sequence of the 146-bp DNA duplex containing an Sp lesion at one of three defined locations, called here Lesion 7 (green), Lesion 9 (orange), and Lesion 12 (purple). (b) Location of the Sp lesions highlighted on the unmodified nucleosome model of Luger and colleagues (PDB ID 1AOI, reference *42*), assuming that the DNA position on the protein core is not changed by the presence of the lesion. All three lesions were placed near the dyad axis of the particle. The histone H3-H4 tetramer is colored in dark grey, while the H2A/H2B dimers are colored in light grey. (c) Proposed location of the Sp lesions shown from the edge of the particle down along the dyad axis. (d, e) Proposed location of the Sp lesions, highlighting their proximity to the histone protein core and (in)accessibility from the solution. Note that the actual DNA bases shown are the control DNA (G, A, and C) and not Sp. Two slightly different conformations, ~1 bp apart, are possible because the model structure is pseudopalindromic.

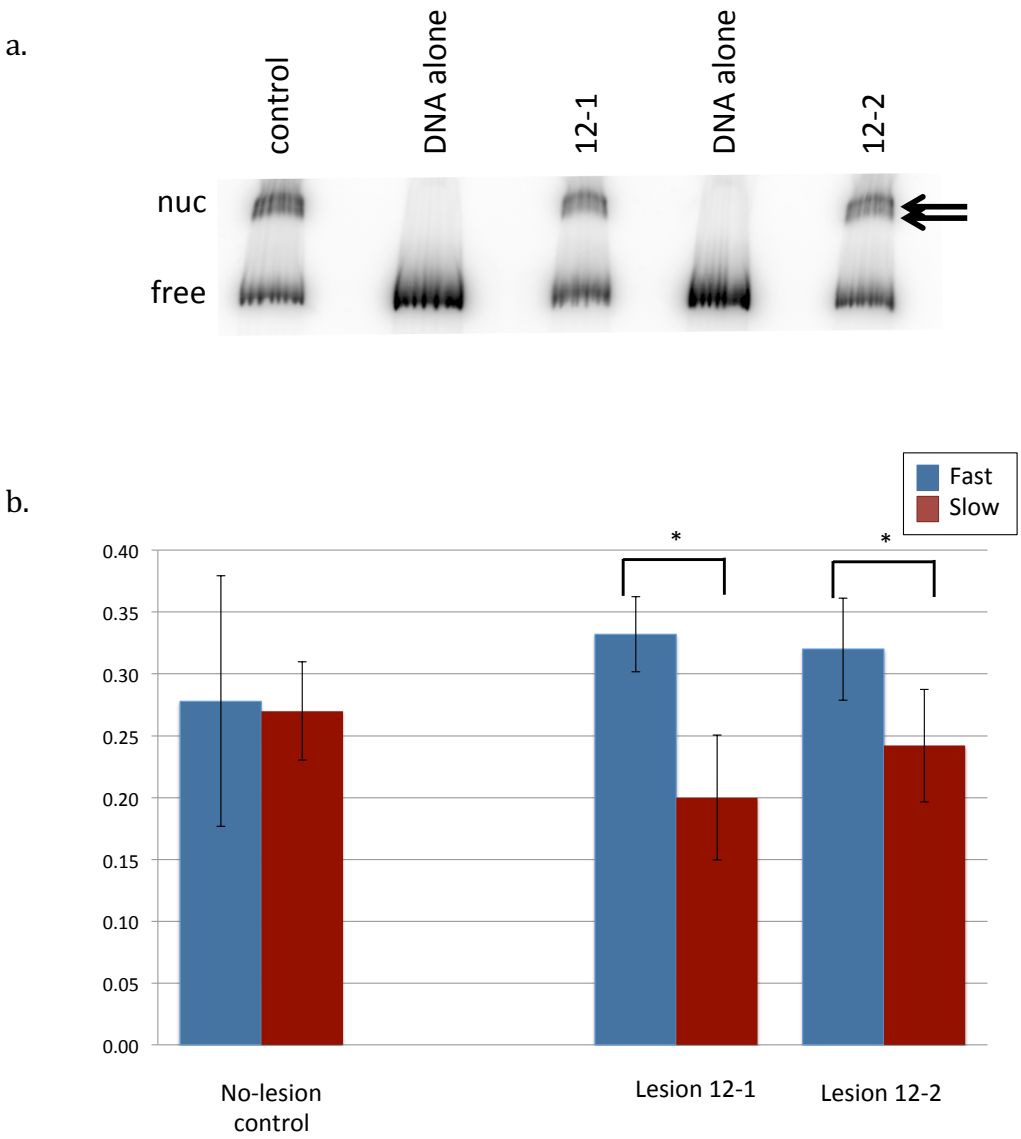

Figure 2: *Stability of Nucleosome Formation Depends upon the Rate of Assembly*. (a) Gel shift showing the results of nucleosome exchange from unlabeled random-sequence DNA to 146-mer duplex under "fast" single dialysis conditions. Nucleosomes were assembled using the control DNA or DNA containing the Sp lesion. DNA duplexes containing the two Sp diastereomers at location 12 were evaluated independently (12-1 and 12-2). The bottom band ("free") contains protein-free DNA and the top bands ("nuc") contain mononucleosomes. Double arrows highlight the double band illustrating the presence of at least two nucleosome conformations. (b) Percent of DNA that forms

nucleosomes under “fast” single dialysis or “slow” double dialysis conditions. The undamaged control forms nucleosomes equally well under either condition, although the variability in the data is diminished under the slower assembly conditions (F-test, >95% confidence). The DNA containing the Sp lesion at location 12 forms fewer nucleosomes when allowed equilibrate more gradually (student’s t test, >95% confidence). Error bars show the standard deviation of the mean (n=5 for all samples, except control double dialysis n=10).

a.

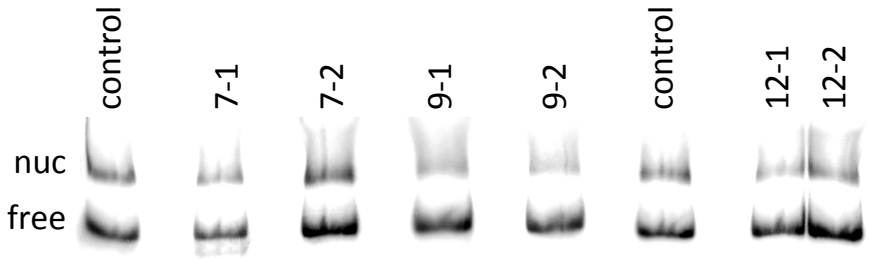

b.

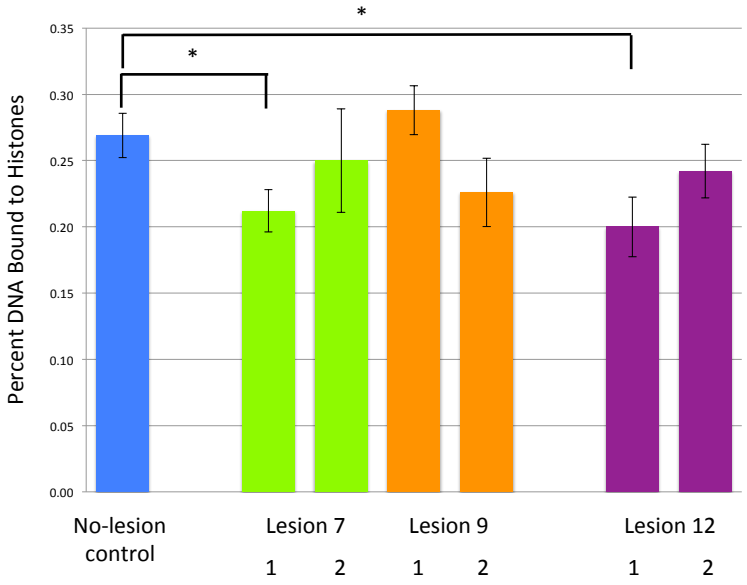

Figure 3: *Stable Lesion-Containing Nucleosomes Are Formed under Slow, Double-Dialysis Conditions*. (a) Gel shift showing the results of "slow" nucleosome exchange from unlabeled random-sequence DNA to 146-mer duplex. All seven possible duplexes are shown, including the control parent DNA and DNA containing both diastereomers of the Sp lesion at locations 7, 9, and 12. Lesion DNA was radiolabeled on the 5' end of the lesion strand; control DNA was 5' end labeled on strand 1 (lane 1) or strand 2 (lane 6). The bottom band ("free") contains protein-free DNA and the top band ("nuc") contains mononucleosomes. (b) DNA containing the Sp lesion forms nucleosomes almost as well as the control. Error bars show the standard error of the mean (control n=10, lesion n=5). Only two duplexes, Lesion 7-1 and Lesion 12-1, bind significantly more weakly than the control (student's t-test, > 95% confidence).

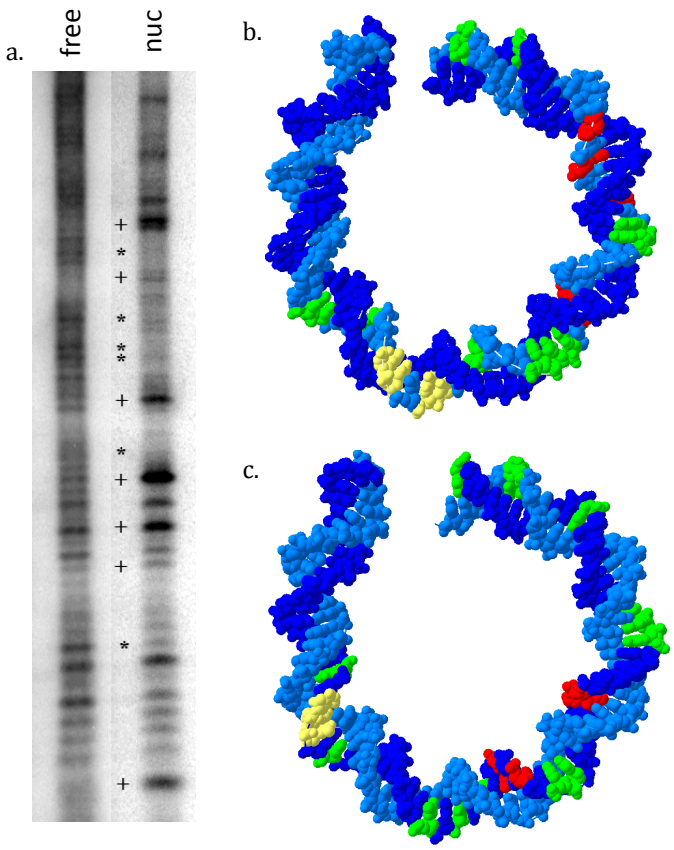

Figure 4: *DNase I Footprinting of Control DNA in Nucleosomes*. (a) DNase I cleavage of bare and nucleosomal control DNA duplexes. The + symbol indicates a location of relatively increased cleavage in the nucleosomal DNA, while * indicates areas of relatively diminished cleavage. Note that the cleavage in the nucleosomal DNA is globally lower than in the bare DNA, both due to shielding by histones and to the presence of unlabeled chicken DNA; both nuclease concentration and visual contrast have been increased in the nucleosomal sample to compensate. (b,c) Changes in DNase I cleavage mapped to the model nucleosome upon which this 146 base pair sequence is loosely based (PDB ID 1AOI, reference *42*). The histone octamer has been removed for clarity. Regions of strong cleavage are colored green, weak cleavage is colored yellow, and absent or drastically reduced cleavage is red. No data are available where the DNA is colored blue. The most robustly cleaved regions correlate with locations where the minor groove is open to the nuclease and the backbone points outward; regions of diminished or absent cleavage point inward toward the octamer.

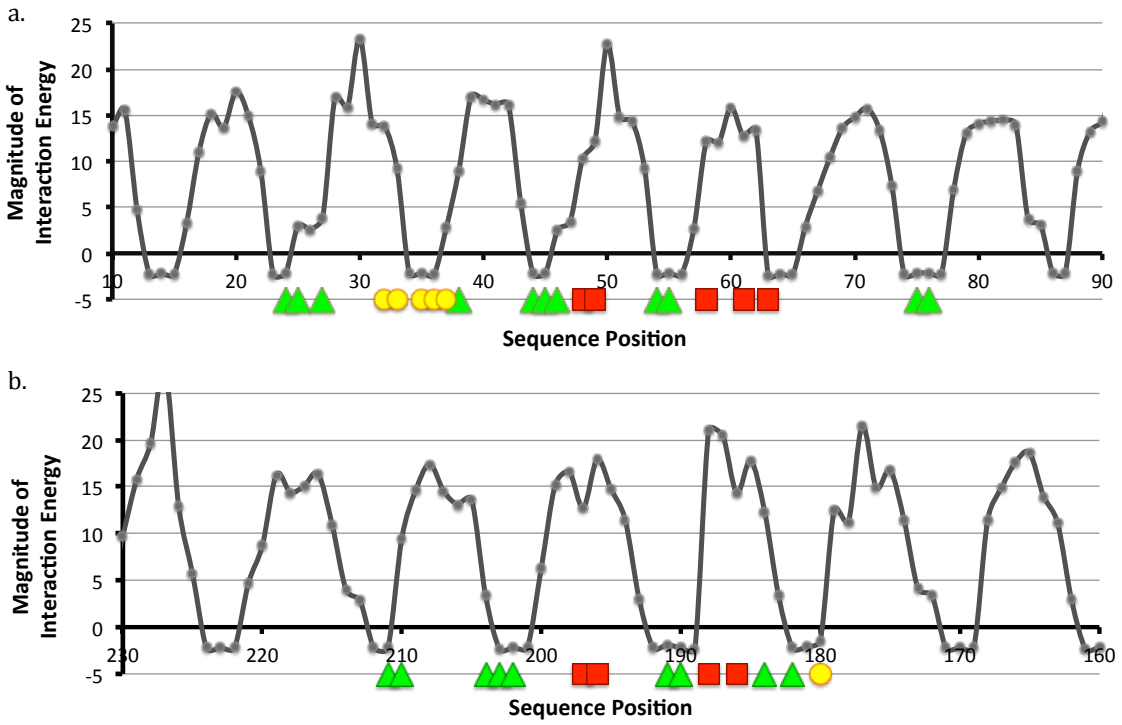

Figure 5: *Computationally Predicted Regions of DNase I Accessibility and Cleavage.* In order to determine where the DNase I would be expected to cleave the model nucleosome structure, the energetic stability of DNAse I-nucleosome complexes was evaluated at every position of the endonuclease along (a) strand 1 and (b) strand 2 of the undamaged 146-base pair DNA duplex. In order to display the large range of interaction energies, y-values represent the $\log_{10}$ of the absolute value of the interaction energies (in kcal/mol). Signs were retained so that negative energies correspond to energetically favorable complexes, while positive energies reflect steric clashes between the histones and the DNase I. The x axes are calibrated to the base pair nearest the active site histidines. In addition to reiterating the experimentally well-known 10 bp periodicity characteristic of nucleosomes, this model illustrates the relatively small "bite size" of the enzyme, since only ~4 bp are accessible for cleavage on each strand as it passes the outside of the nucleosome core particle. At the bottom of each graph are the positions of

experimentally-observed DNase I cleavage on our 146 bp sequence. As in figure 4, regions of strong cleavage are colored green, weak cleavage is colored yellow, and absent or drastically reduced cleavage is red. Generally the experimentally-determined DNase I cleavage lines up well with the modeled negative interaction energies, and the small discrepancies do not show a consistent 5' or 3' trend that would indicate a different rotational or translational position from the model.

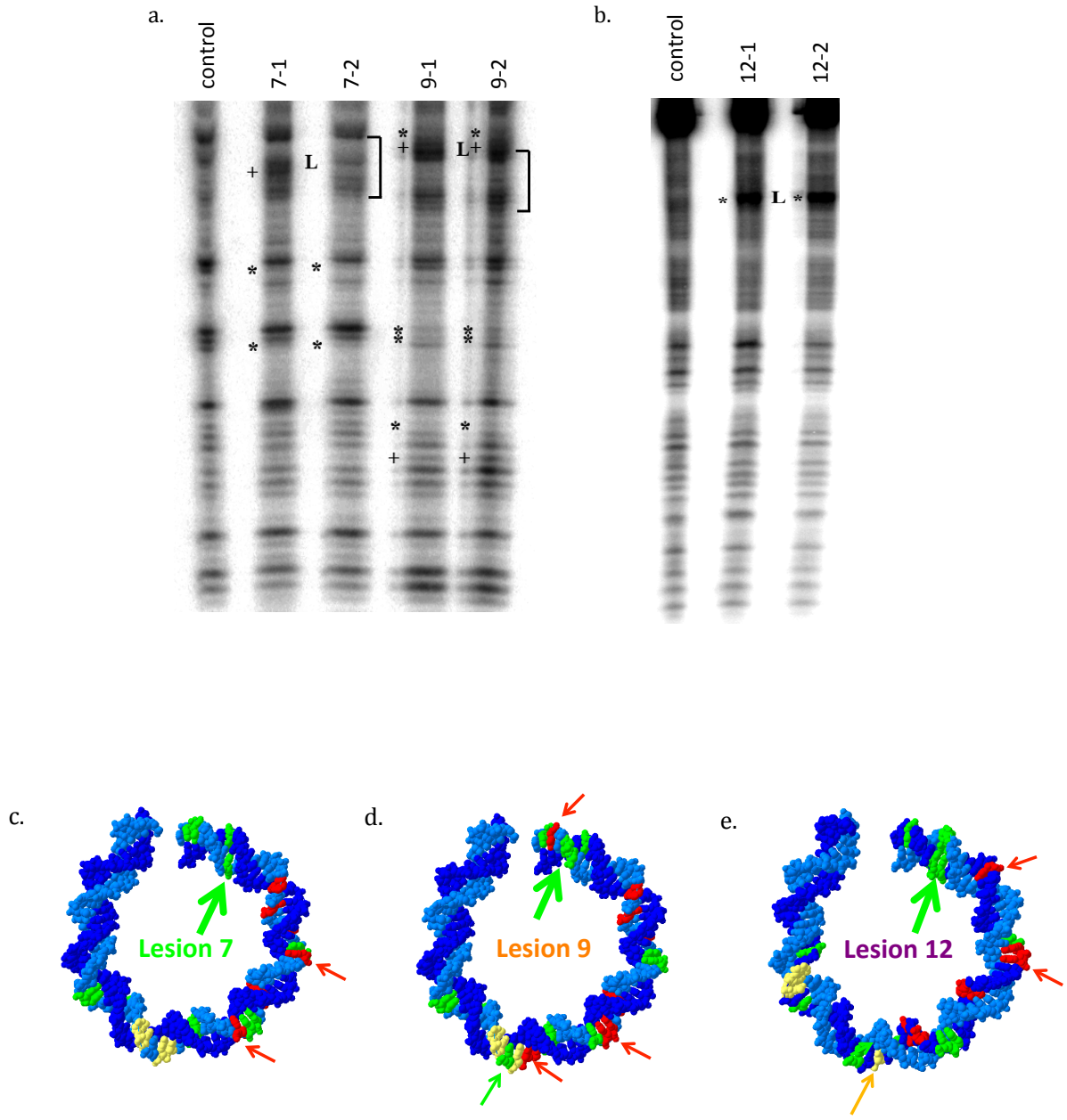

Figure 6: *DNase I Footprinting of Nuclesomes Containing Site-Specifically Incorporated Sp Lesions.* (a) Footprinting analysis of Lesions 7 and 9 and control DNA under double dialysis conditions. Globally, the five samples are quite similar, but some small differences are seen between the two different lesion positions, although not between diastereomers placed in the same location. Bands that are missing relative to the control

are marked with asterisks (*); bands augmented relative to the control are indicated with plus signs (+). Location of the lesions are highlighted with the letter L. The brackets have been added to highlight how the pattern of cleavage is shifted by ~3-4 base pairs between the two lesion positions. (b) Footprinting analysis of Lesion 12 and control DNA under double dialysis conditions. All three samples are essentially identical except for the strong band around the lesion (marked L and *). (c-e) Summary of DNase I footprinting results for DNA containing Sp lesions at locations 7, 9, and 12 superimposed on the structure of the nucleosome core particle DNA with the proteins removed for clarity. Since each pair of diastereomers behaved identically with respect to footprinting, only one picture is shown for each lesion location. Regions of strong cleavage are colored green, weak cleavage is colored yellow, and absent or drastically reduced cleavage is colored red. Since most of the cleaved bases are the same as in the control (Fig. 4bc), red and green arrows highlight locations where the pattern of cleavage is different than the control. Large green arrows correlate with the location of the lesions in each case. For lesion 12, changes in footprints distal from the lesion were observed only under single dialysis conditions.